Self-consistent chaotic transport in a high-dimensional mean-field Hamiltonian map model

D. Martínez-del-Río[◇*], D. del-Castillo-Negrete[⋆†], A. Olvera[◇‡], R. Calleja[◇§]

[◇] IIMAS-UNAM, Mexico, D.F. 04510

[⋆] Oak Ridge National Laboratory, Oak Ridge, Tennessee 37831-8071

Abstract

Self-consistent chaotic transport is studied in a Hamiltonian mean-field model. The model provides a simplified description of transport in marginally stable systems including vorticity mixing in strong shear flows and electron dynamics in plasmas. Self-consistency is incorporated through a mean-field that couples all the degrees-of-freedom. The model is formulated as a large set of N coupled standard-like area-preserving twist maps in which the amplitude and phase of the perturbation, rather than being constant like in the standard map, are dynamical variables. Of particular interest is the study of the impact of periodic orbits on the chaotic transport and coherent structures. Numerical simulations show that self-consistency leads to the formation of a coherent macro-particle trapped around the elliptic fixed point of the system that appears together with an asymptotic periodic behavior of the mean field. To model this asymptotic state, we introduced a non-autonomous map that allows a detailed study of the onset of global transport. A turnstile-type transport mechanism that allows transport across instantaneous KAM invariant circles in non-autonomous systems is discussed. As a first step to understand transport, we study a special type of orbits referred to as sequential periodic orbits. Using symmetry properties we show that, through replication, high-dimensional sequential periodic orbits can be generated starting from low-dimensional periodic orbits. We show that sequential periodic orbits in the self-consistent map can be continued from trivial (uncoupled) periodic orbits of standard-like maps using numerical and asymptotic methods. Normal forms are used to describe these orbits and to find the values of the map parameters that guarantee their existence. Numerical simulations are used to verify the prediction from the asymptotic methods.

[*]dmr@mym.iimas.unam.mx

[†]delcastillod@ornl.gov

[‡]aoc@mym.iimas.unam.mx

[§]calleja@mym.iimas.unam.mx

1 Introduction

There are many problems in physics and the applied sciences where transport plays an important role. Some examples include the dispersion of pollutants in the atmosphere and the oceans, the efficiency of mixing in chemical reactions, the magnetic confinement of fusion plasmas, and vorticity mixing in fluids among others. The study of transport can be classified in two groups: passive and active transport. In the case of passive transport, the elements which are transported do not modify the velocity field of the flow while in the active case, the advected field determines the velocity field through a self-consistent feedback mechanism.

In the present paper, we focus on active transport. The study is based on a simplified model of self-consistent transport in marginally stable systems including vorticity mixing in strong shear flows and electron dynamics in plasmas. The model, originally presented in Ref. [5] and later on studied in Ref. [3], consists of a large set of N mean-field coupled standard-like area-preserving twist maps in which the amplitude and phase of the perturbation (rather than being constant) are dynamical variables. An important part of our methodology is based on the use of normal form methods to describe the evolution of the dynamical variables of the system.

The rest of this paper is organized as follows. Section 2 presents a brief summary of the model and some results originally contained in Ref. [5] that will be used in the present work. In Sec. 3, we study the asymptotic behavior of numerical simulations of the self-consistent map model and in particular the formation of coherent structures. To study these structures, we introduce a reduced transport map model that mimics the asymptotic behavior and that can be interpreted as an uncoupled system in an external oscillatory field. Large iterations of this map are computed for particular sets of initial conditions to show that global diffusion can occur as a result of the oscillation of the perturbation parameter. In Sec. 4, we study the properties of periodic orbits in the self–consistent map and introduce an asymptotic procedure to find a particular kind of periodic orbits that we name sequential periodic orbits. In Sec. 5 we present a simple example illustrating how these sequential periodic orbits can be computed using normal forms and present the relationships between the parameters of the map that should be satisfied for these orbits to exits. The values of the parameters of the sequential periodic orbits obtained by numerical continuation methods are compared with the normal forms results. It is also shown that these numerical and asymptotic results agree up to machine precision. Section 6 present the conclusions.

2 Hamiltonian mean field model of self-consistent transport

The advection-diffusion equation

$$\partial_t \zeta + \mathbf{V} \cdot \nabla \zeta = D \nabla^2 \zeta \,, \tag{1}$$

where ζ is an advected scalar, $\mathbf{V}$ is the velocity field, and D is the diffusivity is one of the fundamental models to study transport in the case of incompressible ($\nabla \cdot \mathbf{V} = 0$) velocity fields. Restricting attention to 2-dimensions, and introducing the stream-function ψ,

$$\mathbf{V} = \hat{\mathbf{z}} \times \nabla\psi \,, \tag{2}$$

Eq. (1) can be written as

$$\partial_t \zeta - (\partial_y \psi)\, \partial_x \zeta + (\partial_x \psi)\, \partial_y \zeta = D\nabla^2 \zeta \,. \tag{3}$$

Broadly speaking, there are two different classes of transport problems. In the case of *passive transport*, ζ, evolves without affecting the velocity field, $\mathbf{V}$. A typical example is the transport of low concentration pollutants in the atmosphere and the oceans. In the case of *active transport*, ζ determines $\mathbf{V}$ through a dynamical self-consistency constraint of the form $\mathcal{F}(\zeta, \mathbf{v}) = 0$ involving an integral and/or differential operator. A paradigmatic example is the 2-dimensional Navier-Stokes equation for an incompressible fluid. In this case, ζ in Eqs. (1) and (3) denotes the fluid vorticity that is self-consistently coupled to the velocity field according to the constrain

$$\zeta = (\nabla \times \mathbf{V}) \cdot \hat{\mathbf{z}} = \nabla^2 \psi \,. \tag{4}$$

Active transport problems, are intrinsically nonlinear and as a result, harder to study than passive transport problems. For example, the well-known challenges in understanding fluid turbulence reside in the nonlinearity in Eqs. (3)-(4). It is thus of significant interest to develop simplified models that capture the basic elements of the self-consistent coupling within a relatively simple mathematical setting. One of these simplified descriptions is the Single Wave Model (SWM) originally proposed in plasma physics [15, 4] and used to study self-consistent transport in marginally stable fluids in the presence of strong shear flows [5]. In general, the stream-function ψ has a complicated spatio-temporal dependence. However, in the SWM, ψ is assumed to have the relatively simple form

$$\psi = -\frac{1}{2} y^2 + a(t)\, e^{ix} + a^*(t) e^{-ix}, \tag{5}$$

and the vorticity stream-function self-consistent coupling in Eq. (4) reduces to

$$\frac{da}{dt} - iUa = \frac{i}{2\pi} \int e^{-ix} dx \int \zeta(x, y, t)\, dy \,, \tag{6}$$

where $a = a(t)$ is in general complex, and U is a constant real parameter. That is, whereas in the Navier-Stokes equation the stream-function has a general spatio-temporal dependence

that is determined at each instant of time by solving the Poisson equation in (4), in the SWM the spatial dependence of the stream-function is given and self-consistency only enters when one determines the temporal dependence of ψ though the amplitude $a(t)$ according to the ordinary differential equation in (6). According to Eq. (2), in the SWM the velocity field consists of a linear component in the x-direction and a traveling-wave component in the y-direction, i.e. $\mathbf{V} = y\mathbf{i} + \mathrm{Re}[ia(t)e^{ix}]\,\mathbf{j}$, where Re denotes the real part.

Despite its relative mathematical simplicity, the SWM is able to capture important dynamics of the full Navier-Stokes equation. In particular, as Fig. 1 from Ref. [5] shows, the SWM exhibit the standard Kelvin-Helmholtz instability leading to the formation of the familiar cats' eyes vorticity structure found in unstable shear flows. The result in Fig. 1 was obtained from the direct numerical integration of Eqs. (1) and (6) with $D = 0.001$, $U = -1$, and initial condition:

$$\zeta(x, y, t = 0) = e^{-y^2/2}\,[1 - 0.2\,y\,\cos(x)]. \tag{7}$$

Although for the sake of simplicity we have stressed the fluid-dynamics interpretation of the SWM, it is important to reiterate that as discussed in Refs. [4, 5, 6] the SWM has its origins in plasma physics and it can be equally applied to the study of electron dynamics in a Vlasov-Poisson plasma in a neutralizing ion background. In this case, ζ corresponds to the single-particle electron distribution function, ψ is the electrostatic potential, the vorticity equation becomes the Vlasov equation, and the (x, y) variables correspond to the (x, u)-phase space variables.

To reformulate the SWM as a finite (but arbitrarily large) degrees-of-freedom Hamiltonian dynamical system, we assume from now on $D = 0$ and introduce the point-vortex representation

$$\zeta(x, y, t) = 2\pi \sum_{j=1}^{N} \Gamma_j\,\delta[x - x_j(t)]\,\delta[y - y_j(t)], \tag{8}$$

where $(x_k(t), y_k(t))$ denote the Lagrangian trajectories of the $k = 1, 2, ...N$ point vortices with intensities Γ_k. In this case, it can be shown that Eqs. (3), (5) and (6) imply the following set of Hamiltonian differential equations determining $(x_k(t), y_k(t))$

$$\frac{dx_k}{dt} = \frac{\partial H}{\partial y_k}\,, \qquad \frac{dy_k}{dt} = -\frac{\partial H}{\partial x_k}, \tag{9}$$

where the Hamiltonian is

$$H = \sum_{j=1}^{N} \left[\frac{1}{2}y_j^2 - a(t)e^{ix_j} - a^*(t)e^{-ix_j}\right], \tag{10}$$

and the function $a = a(t)$ is determined from

$$\frac{da}{dt} - iUa = \frac{i}{N}\sum_{j=1}^{N} \Gamma_j \, e^{-ix_j} \,, \tag{11}$$

which is the point-vortex representation of the SWM self-consistent vorticity stream-function relation in Eq. (6). The Hamiltonian model in Eq. (9) is a mean field model in the sense that the dynamics of the particles (x_k, y_k) is determined by the time dependent field $a(t)$ which according to Eq. (11) depends on the mean properties of the particles' positions.

Defining

$$a = \sqrt{J}\, e^{-i\theta}, \qquad p_k = \Gamma_k \, y_k, \tag{12}$$

equations (9) and (11) can be written as a full $N+1$-degrees of freedom Hamiltonian system

$$\frac{dx_k}{dt} = \frac{\partial \mathcal{H}}{\partial p_k}, \qquad \frac{dp_k}{dt} = -\frac{\partial \mathcal{H}}{\partial x_k}, \tag{13}$$

$$\frac{d\theta}{dt} = \frac{\partial \mathcal{H}}{\partial J}, \qquad \frac{dJ}{dt} = -\frac{\partial \mathcal{H}}{\partial \theta}. \tag{14}$$

where,

$$\mathcal{H} = \sum_{j=1}^{N} \left[\frac{1}{2\Gamma_j} p_j^2 - 2\Gamma_j \sqrt{J} \cos(x_j - \theta) \right] - UJ. \tag{15}$$

The last step to construct the map model is to perform a time discretization of Eqs. (13) and (14) to obtain the self-consistent standard map model originally proposed in Ref. [5],

$$x_k^{n+1} = x_k^n + y_k^{n+1} \tag{16a}$$

$$y_k^{n+1} = y_k^n - \kappa^{n+1} \, \sin(x_k^n - \theta^n) \tag{16b}$$

$$\kappa^{n+1} = \sqrt{(\kappa^n)^2 + (\eta^n)^2} + \eta^n \tag{16c}$$

$$\theta^{n+1} = \theta^n - \Omega + \frac{1}{\kappa^{n+1}} \frac{\partial \eta^n}{\partial \theta^n} \tag{16d}$$

where $k = 1, 2, \ldots, N$, $x_k^n, \theta_n \in [0, 2\,\pi)$, $y_k^n, \kappa^n \in \mathbb{R}$, $\Omega = U\tau$ and the η^n is defined as:

$$\eta^n := \sum_{k=1}^{N} \gamma_k \, \sin(x_k^n - \theta^n), \tag{17}$$

where τ is the discretization time step. The map in Eqs. (16) is a $2N+2$ dimensional map with $N+1$ parameters. The N parameters, γ_k, represent the intensities of the point vortices, and the constant parameter Ω is related to the parameter U in the SWM.

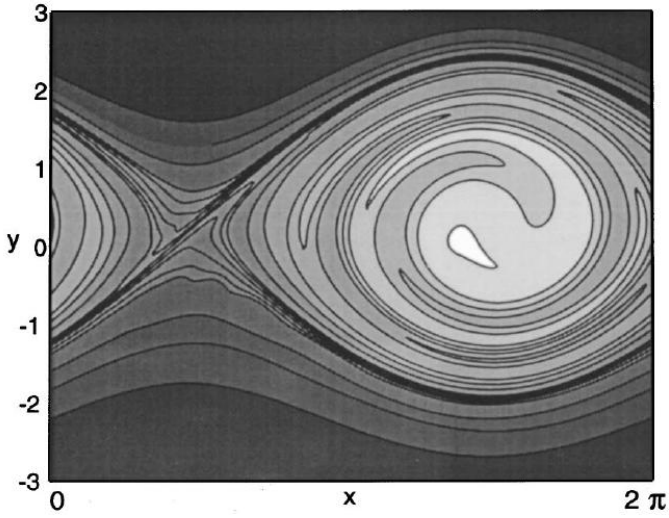

Figure 1: Cat's eye formation and vorticity mixing in the single wave model, Eqs. (3), (5) and (6), with initial conditions in Eq. (7). The gray scale denotes the vorticity values with white corresponding to $\zeta = 1$ and dark gray corresponding to $\zeta = 0$ [After Ref. [5]].

Note that Eqs. (16a)-(16b) have the structure of the well-known symplectic standard map

$$x^{n+1} = x^n + y^{n+1} \tag{18a}$$

$$y^{n+1} = y^n - \varepsilon \sin(x^n - \phi) \tag{18b}$$

with constant, fixed perturbation ε, and phase ϕ (which is usually taken equal to zero). However, in the self-consistent map, the perturbation parameter, κ^n, as well as the phase, θ^n, depend on the iteration, n, and their dynamics is dictated by Eqs. (16c)-(16d) which are the discrete map version of the self-consistent SWM coupling in Eq. (11). Although Eqs. (16c)-(16d) do not define a symplectic transformation, they can be rewritten as a symplectic (although implicit) map in the mean field degrees of freedom [5]. The analogy with the standard map allows us to interpret the map in Eqs. (16a)-(16b) as N coupled oscillators through their phase and amplitudes by the *mean field* in Eqs. (16c)-(16d). We will take advantage of these similarities not only to identify the equations of the map, but also in its perturbation analysis. Note that in the limit $\gamma_k \to 0$ in Eq. (17), the oscillators in (16) depending on θ^0 and Ω decoupled and their equations simply correspond to N copies of the standard map.

3 Coherent structures and transport

The evolution of the self-consistent map in Eqs. (16) has been studied for different initial conditions. Figures 2 and 3 show the results of a simulation of $N = 13,440$ coupled maps with initial conditions $\{(x_k^0, y_k^0)\}$ uniformly distributed on the region $[0, 2\pi] \times [-0.3, 0.3]$ in the (x, y) plane and $\gamma_k = 3 \times 10^{-6}$ for $k = 1, \ldots N$. The initial condition of the mean-field was $\kappa^0 = 10^{-4}$ and $\theta^0 = 0$, and we assumed $\Omega = 0$.

The simulations show that the self-consistent map reproduces the coherent structures observed in the single wave model (Figure 1). In particular, while a group of particles exhibit coherent behavior trapped in the center of the cat's eye, those particles located in the separatrix exhibit a strong dispersion.

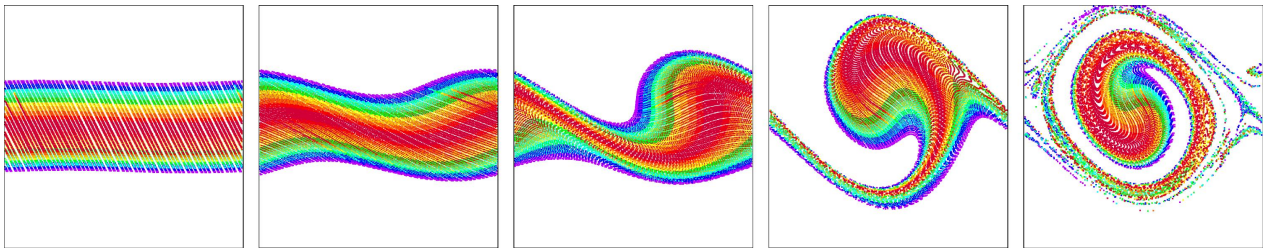

Figure 2: Time evolution of the self-consistent map in Eq. (16) with $N = 13440$ initial conditions uniformly distributed in $[0, 2\pi] \times [-0.3, 0.3]$ with $\kappa^0 = 10^{-4}$, $\gamma_k = 3 \times 10^{-6}$, $\theta^0 = 0$ and $\Omega = 0$. The frames show the instantaneous coordinates of the N initial conditions, at $n = 2, 6, 12, 20$ and 66 in the region $[0, 2\pi] \times [-0.8, 0.8]$ of the (x, y) plane. The colors label the y-coordinate of the initial condition, with red denoting y_k^0 close to $y = 0$ and blue further away.

The evolution of the mean field is represented by the variables (κ^n, θ^n), which are shown in Fig. 3. The behavior of κ^n starts with a fast growth until it achieves a maximum value, after that, the κ^n oscillates around a mean value $\bar{\kappa}$ and the amplitude of oscillation is bounded by $\Delta\,\kappa$. A similar situation is observed with the behavior of $\vartheta^{n+1} = \theta^{n+1} - \theta^n$. Different types of dynamics, including cases in which the mean field decays to zero or saturates at a constant fixed value can be found in Refs. [1, 3] for similar self-consistent maps. Note that in Fig. 3, κ^n does not reach the critical value $\kappa_c = 0.971635406$, which is the value of the parameter κ which corresponds to the destruction of the invariant circle with rotation number equal to the *golden mean*[1] of the standard map [9, 12]. For any $\kappa < \kappa_c$ there is no global diffusion in the standard map because of the existence of invariant circles, that give rise to barriers in phase space. The existence or non-existence of global diffusion in the self-consistent map depends in a nontrivial way on the dynamics of κ^n. On a more fundamental level, the observed rapid

[1]The last invariant circle not homotopic to a point. It must be noted that due the choice of scale of the map, the rotation number is $\omega = 2\pi\gamma$, instead of the golden mean: $\gamma = \frac{\sqrt{5}-1}{2}$.

growth of κ^n for a given initial condition is closely related to the linear stability properties of the corresponding initial condition in the single wave model. In particular, Ref. [4] presents the necessary and sufficient conditions for the linear stability (i.e., exponential growth of the mean field amplitude) of a given initial condition in the context of the continuous, $N \to \infty$ limit. These ideas might help understand the conditions for the growth of κ^n. However, one must be careful before drawing conclusions as the self-consistent map model discussed here is obtained by simplifying drastically the single wave model by approximating the continuous limit when $N \to \infty$.

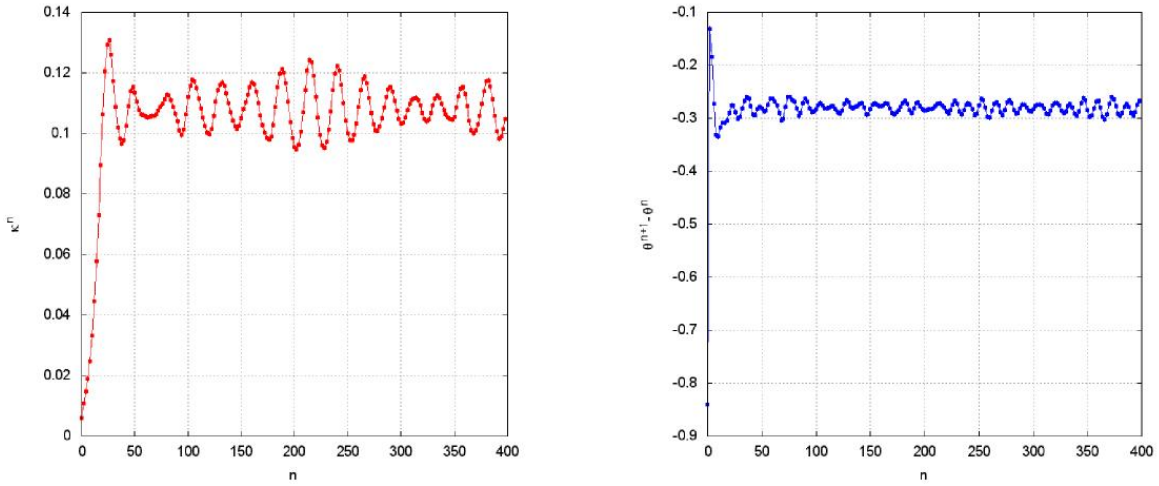

(a) (b)

Figure 3: Time evolution of the mean-field variables in the self-consistent map in Eq. (16) with initial conditions taken in a uniform grid in $[0, 2\pi] \times [-0.3, 0.3]$ with $N = 13440$, $\kappa^0 = 10^{-4}$, $\gamma_k = 3 \times 10^{-6}$, $\theta^0 = 0$ and $\Omega = 0$. κ^n is shown in (a) and $\vartheta^{n+1} = \theta^{n+1} - \theta^n$ in (b).

Perhaps contrary to the intuition, it is observed that global diffusion exists even when $\bar{\kappa} < \kappa_c$. It is also worth mentioning that when the *instantaneous* coordinates (x_k^n, y_k^n) of each degree-of-freedom are plotted on the same plane like in Fig. 2, the amplitude and shape of the cat's eye structure is in good agreement with the invariant manifolds emanating from the hyperbolic fixed point of the standard map calculated with a perturbation parameter equal to the *instantaneous* value of κ^{n+1}. This gives rise to the following question: What is the mechanism that allows the diffusion across the invariant curves on the self-consistent map? In Figure 4 we observe the formation, for relatively small times, of the macro particle coherent structure trapped around the elliptic fixed point, and at the same time we have the formation of the heteroclinic tangle responsible for the high mixing region around the separatrix of the cat's eye.

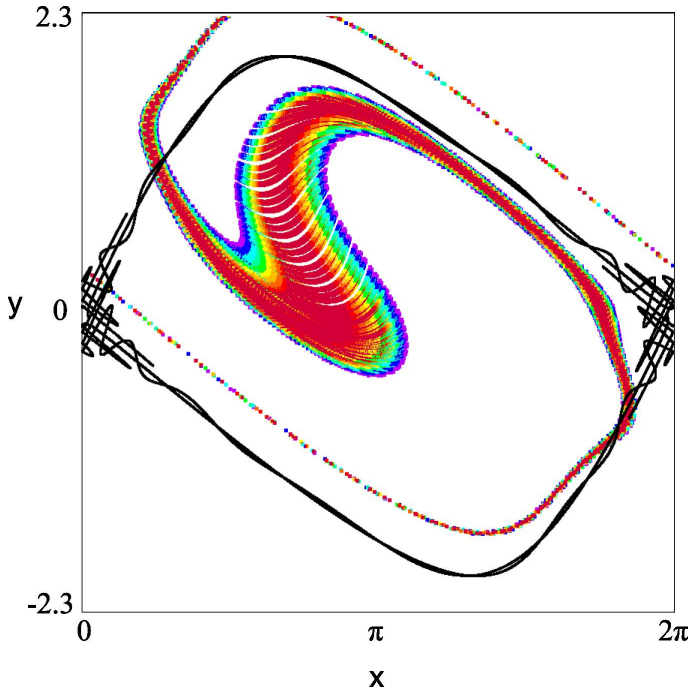

Figure 4: Plot of the projected phase space coordinates (x_i, y_i) on the (x, y)-plane of a simulation of the self-consistent map in Eq. (16) in the oscillatory κ regimen. Also shown in black is the heteroclinic tangle generated by the unstable invariant manifold of the hyperbolic fixed point of the standard map with perturbation parameter equal to κ^n. The initial conditions are the same as those in Fig. 2, except that to enhance the heteroclinic tangle the higher values $\kappa^0 = 0.005$ and $\gamma = 0.0005$ were used.

To address this question, and motivated by the observed oscillation of κ^n, we propose the following non-autonomous map consisting of two copies of the standard map applied sequentially with alternating values of κ,

$$\begin{aligned} y^{n+1} &= y^n - \kappa^n \sin x^n \\ x^{n+1} &= x^n + y^{n+1} \end{aligned} \qquad \text{where} \qquad \kappa^n = \begin{cases} \kappa_1 & \text{if } n \text{ is odd} \\ \kappa_2 & \text{if } n \text{ is even} \end{cases} \tag{19}$$

Without loss of generality, we will assume that κ_2 is greater than κ_1.

To explore the onset of global diffusion for values of κ_1 and κ_2 less than κ_c, we considered a set of N initial conditions uniformly distributed in the region $[0, 2\pi] \times [0, y_{\max}]$ and the map is iterated n times, with n less than some given maximal value M. We then found the number of initial conditions that reached the semi-space $y > y_{\max} + 2\pi$. In turn, this means that one orbit could pass through the invariant circles which exist in the standard map with κ_1 and κ_2 less than κ_c. Figure 5 shows the percentage of initial orbits that reached

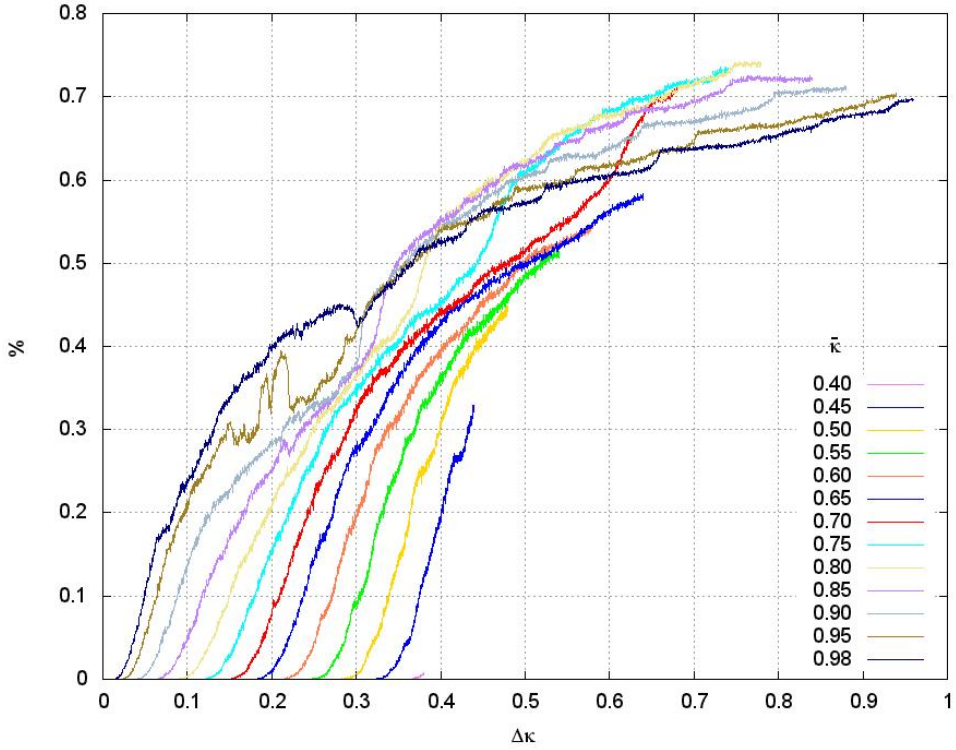

Figure 5: Onset of global transport in the non-autonomous map (19) for different values of $\bar{\kappa} = (\kappa_1 + \kappa_2)/2$. The x-axis corresponds to the difference $\Delta\kappa = \kappa_2 - \kappa_1$ for a fixed value of $\bar{\kappa}$. The y-axis corresponds to the percentage of initial conditions, (x_k^0, y_k^0), taken from a 100×100 regular partition of the rectangle $[0, 2\pi] \times [0, \pi/5]$, that escape due to global transport in the sense that after $M = 100,000$ iterations satisfy $y_k^M \geq \pi/5 + 2\pi$.

the semi-space $y > y_{\max} + 2\pi$ for a given κ_1 and κ_2. For convenience we show the results as function of $\Delta\kappa = \kappa_2 - \kappa_1$ and $\bar{\kappa} = \frac{\kappa_1 + \kappa_2}{2}$. Note that in most cases $\bar{\kappa}$ is lower than κ_c and yet there are cases of global diffusion even when $\kappa_1 < \kappa_2 < \kappa_c$. This results provide numerical evidence of the existence of global diffusion. However, as shown in Fig. 5 there are also cases with no diffusion, a result consistent with Moser's theorem [14] that ensures that for values of κ_1 and κ_2 sufficiently small and for which the twist condition is satisfied, the map (19) should have invariant circles that forbid global transport.

According to Birkhoff's theorem, an invariant circle is the graph of a function $y = f(x)$ and the position of this curve in the (x, y) plane is determined by the value of κ [12]. As shown in Fig. 6, the shape and position of invariant curves with a given rotation number for $\kappa_1 \neq \kappa_2$ in general do not coincide, and the set of points located between these two curves can move upward and downward when we iterate the map (19). Like in a revolving

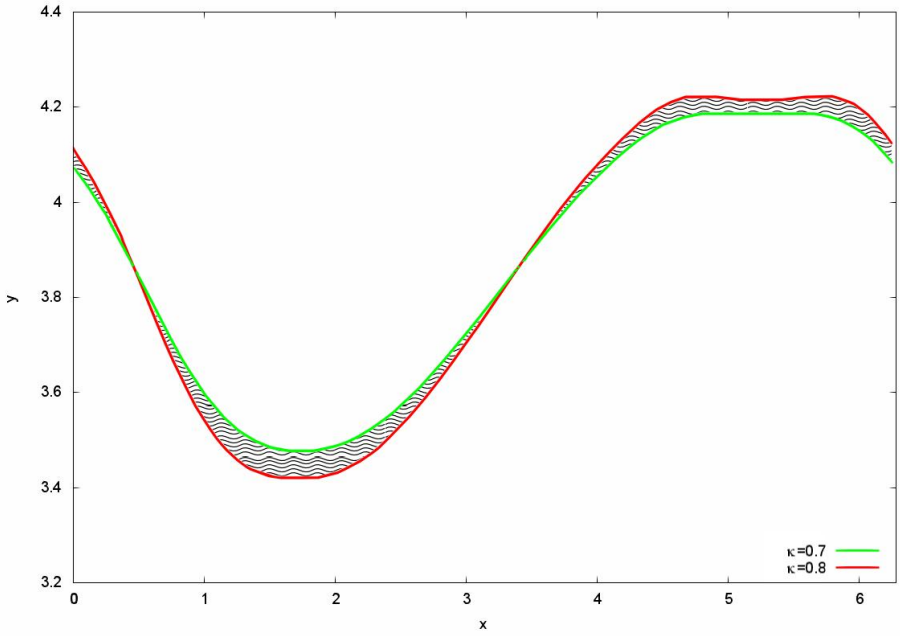

Figure 6: Illustration of the turnstile-type transport mechanism across invariant circles in the non-autonomous standard map. The plot shows the invariant circles (approximated using the parametrization method in Ref. [2].) with golden mean rotation number in the standard map (18) for two different values of the perturbation parameter $\kappa_1 = 0.7$ and $\kappa_2 = 0.8$. Due to the periodic switching between these two values of κ^n in the non-autonomous standard map in Eq. (19), points in the shaded region can cross the golden mean tori even though the perturbation is below the critical value $\kappa_c = 0.971635406$ for the onset of global transport in the standard map.

door, every two iterations, points between the two invariant circles move across the invariant circles. This turnstile-like type mechanism does not appear for all κ_1 and κ_2. In fact, we can appreciate in Fig. 5 that the probability to jump across the invariant circles goes to zero when $\Delta\,\kappa$ approaches zero. This means that there exist invariant circles for the composed map (19) for small values of $\Delta\,\kappa$.

Note that even if two standard maps with perturbation amplitudes κ_1 and κ_2 do not have common invariant curves, there is no reason to assume that their composition has no invariant curves. To determine the threshold of (κ_1, κ_2) values for which the map (19) exhibits global diffusion more simulations were performed for a wider range of values. To do this, we used the following criterion: if there is an initial condition $y_0 \in [0, y_m]$, with $y_m \in (0, 2\pi)$, for which $y^n > y^* = y_m + 2\pi\ell$ or $y^n \leq y^{**} = -2\pi\ell$, for some $\ell \in \mathbb{N}$ for a given n, then there is global transport, i.e. the system has no invariant circles. Figure 7 shows the minimum value of κ_2 for a given κ_1 such that the simulations satisfy this criterion, for $\ell = 1, 2$. Note that for the case $\ell = 2$ we have increased the number of iterations to

obtain estimates comparable to $\ell = 1$. We emphasize that this criterion assumes that the map is invariant under the transformation $(x_n, y_n) \to (x_n, y_n + 2\pi)$ which is the case of the map under study. We found a symmetrical bifurcation diagram in positive quadrant of the (κ_1, κ_2) parameter space. Points inside the "horn" correspond to cases were none of the initial conditions reached $y*$. In other words, there is not global diffusion for values of κ_1 and κ_2 inside the horn.

It can also be observed in Fig. 7 that the numerically determined thresholds for global transport for parameter values $(\kappa_1, 0)$ and $(0, \kappa_2)$ satisfy to a very good approximation $\kappa_1^* = \kappa_2^* = \kappa_c/2$. This follows directly from the fact that, for the case $(\kappa_1, 0)$, the non-autonomous standard map for every other iteration reduces to

$$x_{n+1} = x_n + 2y_n - 2\kappa_1 \sin(x_n) \tag{20a}$$

$$y_{n+1} = y_n - \kappa_1 \sin(x_n) \tag{20b}$$

Upon the change of coordinates, $\{X = x, Y = 2y\}$, this map becomes the standard map (18) with $\varepsilon = 2\kappa_1$, which as it is well known exhibits global chaos for $\varepsilon = \kappa_c$. An analogous reduction happens for the case $(0, \kappa_2)$. Further details of these calculations will be reported in a forthcoming publication where we also study negative (κ_1, κ_2) values and examine the rotation numbers of the most robust invariant circles.

4 Periodic orbits

As a first step to understanding transport and the formation of coherent structures we present in this section a study of the periodic orbits of the self-consistent map. In particular, we determine the asymptotic value of $\bar{\kappa}$ and $\Delta\,\kappa$ for an special kind of initial conditions and parameter values. To do this, the specific form of the mean field auxiliary variable η^n (17) is taken into account to try to determine which are the sets of initial conditions that correspond to η^n's that are as small as possible.

Finding periodic orbits for high dimensional maps is a complex problem and numerical simulation is in principle the only procedure to estimate the asymptotic behavior of the mean field variables. However, when using simulation it is hard to predict the result from the initial conditions and usually a large number of iterations are needed. In our case, the dimension of the self-consistent map (16) has to be rather big (of order 10^4) so that the system can achieve similar patterns to that of the single-wave model. In practice it is not possible to approach this problem using analytic or asymptotic tools. One possibility is to reduce the complexity of the problem by only taking into account the periodic solutions of the map (16). In general, the structure of periodic solutions determines the behavior of any dynamical system, our goal is to show that periodic orbits are closely related to the mean-field variables (in particular $\bar{\kappa}$ and $\Delta\,\kappa$) and the choice of values of the parameters.

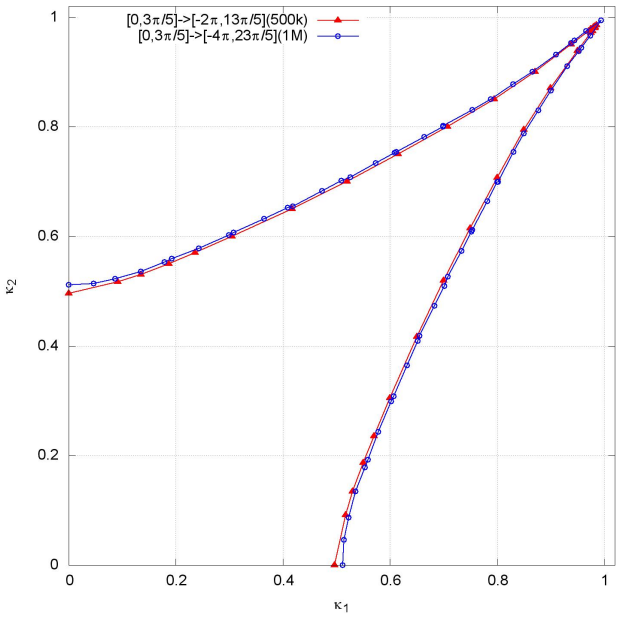

Figure 7: Critical values (κ_1, κ_2) for global transport in the non-autonomous standard map in Eq. (19). The area outside the "horn" corresponds to parameter values for which particles escape in the sense that at least one of 10^4 initial condition uniformly distributed on the rectangle $[0, 2\pi] \times [0, 3\pi/5]$ exhibited a displacement with: (i) $y > 3\pi/5 + 2\pi$ or $y < -2\pi$ after 5×10^5 iterations (red) and (ii) $y > 3\pi/5 + 4\pi$ or $y < -4\pi$ after 10^6 iterations of the map (blue).

In the case of low-dimensional maps, the use of symmetries can greatly simplify the search of periodic orbits [11]. For the self-consistent map, we can simplify the problem by assuming $\gamma_k = \gamma$ constant, for $k = 1, \ldots, N$ in (16c) which implies the following properties:

1. Let $\mathbf{z}$ be a periodic orbit of map (16) with dimension $2N + 2$. If we set the initial condition of this orbit to be,

$$\mathbf{z}^0 = (x_1^0, y_1^0, x_2^0, y_2^0, \ldots, x_N^0, y_N^0, \kappa^0, \theta^0) \quad , \tag{21}$$

   then any permutation of the pairs (x_i^0, y_i^0), for $i = 1, \ldots, N$, produces a new periodic orbit with the same period. This is because the term that couples the standard maps only depends on the average of the variables x_i.

2. For any periodic orbit $\mathbf{z}$ of the map (16) with dimension $2N + 2$, we can increase the dimension of the solution by replicating the orbit $\mathbf{z}$ and reducing the strength of γ by one half. Thus, for any $\mathbf{z}$ given in (21), we can generate a new periodic solution of

dimension $2N$ of the form,

$$\mathbf{z}^0 = (x_1^0, y_1^0, x_2^0, y_2^0, \ldots, x_N^0, y_N^0, x_1^0, y_1^0, x_2^0, y_2^0, \ldots, x_N^0, y_N^0, \kappa^0, \theta^0) \quad ,$$

with the strength of vorticity equal to $\gamma/2$. The dimension of this new orbit is $4N+2$ and the period of the orbits is the same as (21). In this case, since γ is rescaled by a factor of $1/2$, the function η in (16c) preserves the value given when we calculate it at the orbit (21) since we have to sum N terms twice.

With these two properties, we can generate a large set of periodic orbits: starting with low dimensional map corresponding to $N = 1$ and a strength parameter γ, we can find periodic orbits of period M. Using the property 2, the orbit can be replicated s times, such that we get an orbit of dimension 2^s but with reduced strength in the parameter $\gamma' = \gamma/2^s$.

Another possibility is to construct a periodic orbit by imposing that the iteration of each initial condition almost coincides with the previous point in the orbit of the next initial condition. This is, if (x_i^n, y_i^n) is the i-th initial condition and (x_i^{n+1}, y_i^{n+1}) is the next point in the periodic orbit, then $(x_i^{n+1}, y_i^{n+1}) \approx (x_{i+1}^n, y_{i+1}^n)$. We will call this kind of periodic orbits as *sequential periodic orbits* (SPO's). To generate this kind of orbits, we compute a periodic orbit of period τ of the standard map for a fixed value of κ and θ. The iterations of this orbit give the following set of pairs of coordinates:

$$(x_0, y_0) \;\; (x_1, y_1) \;\; \ldots \;\; (x_{\tau-1}, y_{\tau-1}) \quad . \tag{22}$$

With this sequence of points, we construct a periodic orbit of dimension $2\tau + 2$ with period τ for the map (16), with initial condition,

$$(x_0, y_0, x_1, y_1, x_2, y_2, \ldots, x_{\tau-1}, y_{\tau-1}, \kappa, \theta) \quad .$$

For $\gamma = 0$, this orbit follows a sequential pattern, that is, the coordinates (x_i, y_i) in the position i are shifted to the position $i+1$ for each iteration of the map. It is clear that this is not a periodic orbit for $\gamma \neq 0$ because the mean-field variables, κ and θ, are going to change while the orbit is iterated. Nevertheless, this is a good guess for finding a periodic orbit using numerical or asymptotical procedures for small values of γ.

Based on the previous ideas, our numerical procedure to find a periodic orbit of (16) with period τ and dimension $2\tau + 2$ consists of the following steps:

1. For given values of θ and κ, we find a symmetric periodic orbit of period τ of the standard map using the symmetry lines of the map [9].

2. With this orbit, a sequential periodic orbit (22) is formed. For $\gamma = 0$ this is a periodic orbit of the self-consistent map (16).

3. Using a continuation method, the sequential periodic orbit is computed for small values of γ [8] and continued for large values of γ.

4. The dimension of the orbit is then increased using the replication property of the map (16). For each replication, the strength parameter γ is divided by two.

5. The value of the auxiliary variable η^n is small in all iterations due the almost equidistribution on the angular variables x_i^n.

Following this procedure, we can compute periodic solutions for small periods. The convergence of the continuation–method requires adjusting the value of the parameter Ω in (16d), otherwise the variable θ might not converge to a value. After some numerical experiments, we concluded that for the method to converge, Ω should be a function of κ^0. Therefore, we have included Ω in the numerical method as a free parameter which has to be determined by the continuation process.

We proceed in a similar way to determine periodic orbits using a perturbative method. The idea is to compute a sequential periodic orbit in an asymptotic way. We have to begin the process with an integrable map, in our case this map is (16) when the parameter γ and the variable κ^n are zero. For this integrable case, the periodic solution with period q is:

$$\left(x_1^0 = 2\pi\frac{p}{q}, y_1^0 = 2\pi\frac{p}{q}, x_2^0 = 2\pi\frac{2p}{q}, y_2^0 = 2\pi\frac{p}{q}, ..., x_q^0 = 2\pi\frac{qp}{q}, y_q^0 = 2\pi\frac{p}{q}, \kappa^0 = 0, \theta^0 = \theta_0, \right), \tag{23}$$

where p and q are positive integers and θ_0 is a constant. We see that the iteration of this initial orbit has simple dynamics: $x_i^j \to x_j^{i+1} = x_{j+1}^i$, $y_i^j = y_j^{i+1}$, $\kappa^j = 0$ and $\theta^j = \theta_0$, where the variables x and θ are defined in the interval $[0, 2\pi)$. The integrable periodic orbit (23) is the initial point of our asymptotic procedure. The small parameter in our method is γ and the variable κ^j has to be small as well. We also set κ^j to be of order $\mathcal{O}(\gamma)$.

5 Normal forms and sequential periodic orbits.

Normal forms are reduced systems obtained by changes of variables designed to simplify a set of equations [13, 10]. The concept of normal form goes back to Poincaré and for this reason, there are many different approaches for different problems [7]. When the system is written at different scales of a small parameter, it is possible to find relations between the systems dynamics and the parameters. These relations can also be found by performing a high number of simulations and performing parameters correlations, but this can be very time consuming and often not as accurate as the results of an asymptotic method.

The normal form approach that we are interested in, is the one used in [16]. The proposed change of variables is written as an infinite series such that the initial evolution equations

are rewritten as a Poincaré-Lindstedt system ordered by a small parameter. In our case, the small parameter corresponds to the initial value of $\epsilon = \kappa^0$, where γ is also assumed small. Of course, this choice is arbitrary since we are looking for periodic orbits in the map. Therefore we can always take a different choice, for instance κ^1.

A big difference with [16] is that instead of introducing a single change of variables for a 2-dimensional map, for the $2N+2$-dimensional map, a change of variables is proposed for each oscillator (x_k, y_k) with the *a priori* condition that all the oscillators and the mean field (κ, θ) have the same *rational* winding number $\omega = 2\pi p/q$, $p/q \in \mathbb{Q}$. The reason of this condition is that we decrease the effective number of variables needed and we avoid performing an extra change of variables for the *mean field* map. In order to prepare the map (16) in a suitable form, we rewrite the oscillators' equations (16a) and (16b) in the Lagrangian form,

$$x_k^{n+1} - 2x_k^n + x_k^{n-1} = -\kappa^{n+1} \sin(x_k^n - \theta^n) \tag{24a}$$

$$\kappa^{n+1} = \sqrt{(\kappa^n)^2 + (\eta^n)^2} + \eta^n \tag{24b}$$

$$\theta^{n+1} = \theta^n - \Omega + \frac{1}{\kappa^{n+1}} \frac{\partial \eta^n}{\partial \theta^n} \tag{24c}$$

The proposed change of variables for each oscillator is

$$x_k = \zeta + \omega k + g(\zeta + \omega k, \kappa^0), \tag{25}$$

where ω is a given winding number and $g(\phi, \varepsilon)$ is given by

$$g(\phi, \varepsilon) = \sum_{j=0}^{\infty} \varepsilon^j \sum_{m \in \mathbb{Z}} g_{j,m}\, e^{im\phi}. \tag{26}$$

Substituting (25)-(26) in (24a) yields for each oscillator the *same* homological equation[2]:

$$\sum_{j=0}^{\infty} (\kappa^n)^j \sum_{m \in \mathbb{Z}} g_{j,m}\, e^{im\zeta_k^n} c_m = \frac{\sqrt{(\kappa^n)^2 + (\eta^n)^2} + \eta^n}{2i} \left\{ \exp\left(i(x_k^n - \theta^n)\right) - \exp\left(-i(x_k^n - \theta^n)\right) \right\}, \tag{27}$$

where

$$c_m := 2(1 - \cos(2\pi m p/q)), \tag{28}$$

$$\eta^n = \frac{\gamma}{2} \sum_{k'=1}^{N} \left\{ \exp\left(i(x_{k'}^n - \theta^n)\right) + \exp\left(-i(x_{k'}^n - \theta^n)\right) \right\}. \tag{29}$$

[2]The equation still depends on the label k of each oscillator, but it can be absorbed in the angular variable: $\zeta_k := \zeta + \omega k$

To solve (27), we impose a relation between the two *small* parameters [3] γ and κ^0, so the homological equation can be organized hierarchically in terms of a single variable $\varepsilon = \kappa^0$, as in the Poincaré-Lindstedt method. This relation is added in order to have a well ordered set of equations for the perturbation analysis, and it is not a physical constraint that the system must necessarily obey. The lowest order at which the problem can be solved is: $\gamma \propto \kappa^0$ or $\gamma = \alpha\kappa^0$, $\alpha \in \mathbb{R}$. Also, for (29) to be summable at order $\mathcal{O}(1)$, we set the mean value to zero on each change of variables.

From (28), it is obvious that there will be cases were (27) will not be solvable. The terms on the right hand side that can not be eliminated, give the *normal resonant form* of (24a)[4]. In general the normal form has the following structure,

$$x_k^{n+1} - 2x_k^n + x_k^{n-1} = \sum_{\ell=q}^{\infty} \left(\kappa^0\right)^{\ell} \left\{ c_\ell^+(\alpha)\, e^{i\ell\left(\zeta_k^n - \theta^n\right)} + c_\ell^-(\alpha)\, e^{-i\ell\left(\zeta_k^n - \theta^n\right)} \right\}. \tag{30}$$

The next step is to substitute the computed $g(\phi, \varepsilon)$ in the map to find the needed initial conditions and additional parameters to have these *p/q-periodic orbits*, that we will call *sequential periodic orbits*.

After such substitution on the map and its next q iterations, we found that for given κ^0 and α small, the *sequential periodic orbits* exist only for a certain value of the parameter $\Omega = \Omega(\kappa^0, \alpha)$, if the initial conditions of the oscillators are taken *near* the *fixed points*[5]: hyperbolic, elliptic or a mixed type.

To conclude this section we present the steps to compute the first terms of the change of variables $g(\phi, \varepsilon)$ and the resonant normal form for the sequential periodic orbit with period $\tau = 2\pi/3$. We present the calculations done with them to determine the corresponding dependence of Ω on κ^0.

1. We write the zeroth order of the homological equation (27), substituting $(\gamma = \alpha\,\kappa^0)$[6],

$$\sum_{m\in\mathbb{Z}} g_{0,m}\, e^{im\zeta^0} c_m = 0, \tag{31}$$

[3] For the perturbation analysis to work we can assume that both parameters are small. Notice that this assumption is consistent since both parameters can be traced back to the perturbation parameter of the standard map.

[4] Were both equations have been merged into 1, the *lagrangian* representation of a 2-dimensional map.

[5] Actually fixed points for the map iterated q times.

[6] It is important to remind that the upper index 0 is just a reference, the value of γ will not change from iteration to iteration even though the change of variables g and the *normal form* are used to evaluate iterations of the map.

where for this case is,

$$c_k = \begin{cases} 0, & \text{k=3m} \\ 3, & \text{k=3m+1} \\ 3, & \text{k=3m+2} \end{cases} \quad , \quad m \in \mathbb{Z} \tag{32}$$

and we have omitted the sub-index k on ζ_k^n since the value of ζ does not change with k in this case. We have several free parameters that can be used later, but for the moment we set them all to zero, meaning

$$g_{0,m} = 0 \qquad \forall m \in \mathbb{Z}. \tag{33}$$

2. Now we write the next order, (κ^0) of the homological equation,

$$\sum_{k\in\mathbb{Z}} g_{1,k} e^{ik\zeta^0} c_k = \frac{1}{2i}\left(e^{i(\zeta^0-\theta^0)} - e^{-i(\zeta^0-\theta^0)}\right). \tag{34}$$

From which we obtain,

$$g_{1,1} = \frac{1}{6i} e^{-i\theta^0}, \qquad g_{1,-1} = \frac{-1}{6i} e^{i\theta^0}. \tag{35}$$

and set the remaining $g_{1,m}$ to 0.

3. We repeat the process for the following orders.

Up to order $((\kappa^0)^3)$, we compute,

$$g_{2,2} = \frac{1}{36i} e^{-i2\theta^0}, \qquad g_{2,-2} = \frac{-1}{36i} e^{i2\theta^0}, \tag{36}$$

$$g_{3,\pm4} = -\frac{\alpha}{96} e^{\mp 4i\theta^0}, \quad g_{3,\pm2} = \frac{\alpha}{96} e^{\mp 2i\theta^0}, \quad g_{3,\pm1} = \mp\frac{1}{432i} e^{\mp i\theta^0}. \tag{37}$$

We stop at this order due to the existence of the resonant terms,

$$c_3\Big|_0 \; g_{3,\pm3} = \pm\frac{1}{48i} e^{\mp 3i\theta^0} \tag{38}$$

4. Adding these results gives the change of variables[7]

$$\begin{aligned} g(\zeta^0,\kappa^0) \;\; = \;\; & \frac{\kappa^0}{3}\sin(\phi^0) + \frac{(\kappa^0)^2}{18}\sin(2\phi^0) + \frac{(\kappa^0)^3}{216}\sin(\phi^0) \\ & + \frac{\alpha(\kappa^0)^3}{48}\big(\cos(2\phi^0) - \cos(4\phi^0)\big) + \mathcal{O}((\kappa^0)^4), \end{aligned} \tag{39}$$

[7]Where: $\phi^k := \zeta^k - \theta^k$.

and the resonant normal form,

$$\zeta^1 - 2\zeta^0 + \zeta^{-1} = -\frac{(\kappa^0)^3}{24}\sin(3\phi^0) + \mathcal{O}((\kappa^0)^4). \tag{40}$$

5. Substituting (39) and (40) in the map (24), we solve the mean field, in other words, we look for the needed initial conditions and the parameters to have the same period for the variables κ and θ.

   (a) κ^n: Substituting (39) into map in (24b), we obtain,

   $$\kappa^1 = \kappa^0\Big(1 + \frac{\alpha(\kappa^0)^2}{6}\sin(3\phi^0) + O((\kappa^0)^4)\Big), \tag{41}$$

   and substituting in the following iterates yields,

   $$\kappa^3 = \kappa^0 + \frac{\alpha(\kappa^0)^3}{6}\Big(\sin(3\phi^0) + \sin(3\phi^1) + \sin(3\phi^2)\Big) + \mathcal{O}((\kappa^0)^5) \tag{42}$$

   So, the condition to have period 3 in κ^n is,

   $$\sin(3\phi^0) + \sin(3\phi^1) + \sin(3\phi^2) = \mathcal{O}((\kappa^0)^2). \tag{43}$$

   (b) (x^n, y^n): After substituting (40) into (24a) and imposing $\zeta_3 - \zeta_0 - 2\pi = 0$, we obtain a similar condition,

   $$\sin(3\phi^0) + \sin(3\phi^1) + \sin(3\phi^2) = \mathcal{O}(\kappa^0). \tag{44}$$

   (c) θ^n: Substituting (39) and the results for κ^n into the map in (16d), yields a different condition[8],

   $$\begin{aligned}\theta^3 &= \theta^0 - 3\Omega + \frac{3}{2}\alpha\kappa^0 - \frac{\alpha(\kappa^0)^2}{8}\Big[\sum_{j=0}^{2}\mathrm{c}(3\phi_j) + \frac{1}{2}\sum_{j=0}^{2}\mathrm{s}(3\phi_j)\Big] \\ &\quad + \frac{3\alpha(\kappa^0)^3}{324} + \frac{\alpha^2(\kappa^0)^3}{24}[4\mathrm{s}(3\phi^0) + 3\mathrm{s}(3\phi^1) - \mathrm{s}(3\phi^2)] + \mathcal{O}(\alpha(\kappa^0)^4).\end{aligned} \tag{45}$$

[8] Where $\mathrm{s}(\phi) \equiv \sin(\phi)$ and $\mathrm{c}(\phi) \equiv \cos(\phi)$.

The conditions (43), (44) and (45) can only be solved in the general case if we restrict to the fixed points (of the map iterated q times). After the change of variables, $\phi = \frac{2n\pi}{3}$ ($\phi = \frac{(2n+1)\pi}{3}$) corresponds to the linear elliptic (hyperbolic) fixed points at least at order κ^0.

Then (43) and (44) are satisfied and (45) yields,

$$\Omega = \frac{\alpha\kappa^0}{2} - \frac{\alpha(\kappa^0)^2}{8} + \frac{\alpha(\kappa^0)^3}{324} + \mathcal{O}(\alpha(\kappa^0)^4), \tag{46}$$

for linear elliptic *fixed* points and

$$\Omega = \frac{\alpha\kappa^0}{2} + \frac{\alpha(\kappa^0)^2}{8} + \frac{\alpha(\kappa^0)^3}{324} + \mathcal{O}(\alpha(\kappa^0)^4), \tag{47}$$

for linear hyperbolic *fixed* points.

If $\kappa^1 = \sqrt{(\kappa^0)^2 + (\eta^0)^2} + \eta^0 \simeq \kappa^0 + \eta^0 + \mathcal{O}((\eta^0)^2/\kappa^0)$, we can expand $\eta^0 = \gamma \sum \sin(x_k^0 - \theta^0)$ and we substitute x_k^0 from (25), we obtain

$$\kappa^1 - \kappa^0 \simeq \frac{\alpha^2(\kappa^0)^4}{64}. \tag{48}$$

Table 1 shows the change of variables, normal resonant form and $\Omega(\kappa^0)$ relations for two kinds of initial conditions (elliptic and hyperbolic fixed points) for given rotation numbers.

The three examples show that the relation of the asymptotic value of the mean field variables with the parameters of the self–consistent map (16). For each rotation number of the sequential periodic orbit we obtain a specific value of the average of κ and the amplitude of its oscillation. Table 1 shows these values for rotation numbers 1/2, 1/3 and 1/6. The main point is the relation between Ω and κ^0. Fixing the values of the parameters γ and Ω, we can find the average value of kappa, where $\bar{\kappa} = \kappa^0$ by using equations (46) and (47) and the relation $\gamma = \alpha\kappa^0$. The amplitude of the variation of κ is given by $\Delta\,\kappa = \max|\kappa^i - \kappa^0|$, for $i = 1, \ldots, N$, which first approximation is written in (48). This method can be used for any sequential periodic orbits of period τ.

We use our numerical procedure to compute the previous sequential periodic orbits. The first step is to compute a periodic orbit with the same rotation number as the sequential periodic orbit of the standard map (18) with value of the parameter $\kappa = \kappa^0$. This orbit was our initial guess for the numerical approximation of the sequential periodic orbit. In order to have convergence in the Newton method, it is necessary to define Ω as a free parameter, in this way the numerical procedure converges for a specific value of Ω.

The normal forms and the numerical method to find sequential periodic orbits imply an interesting relation between κ^0 and Ω. In order to compare the numerical and the asymptotical methods, we evaluate the relation (46) using the values of κ and Ω obtained from the

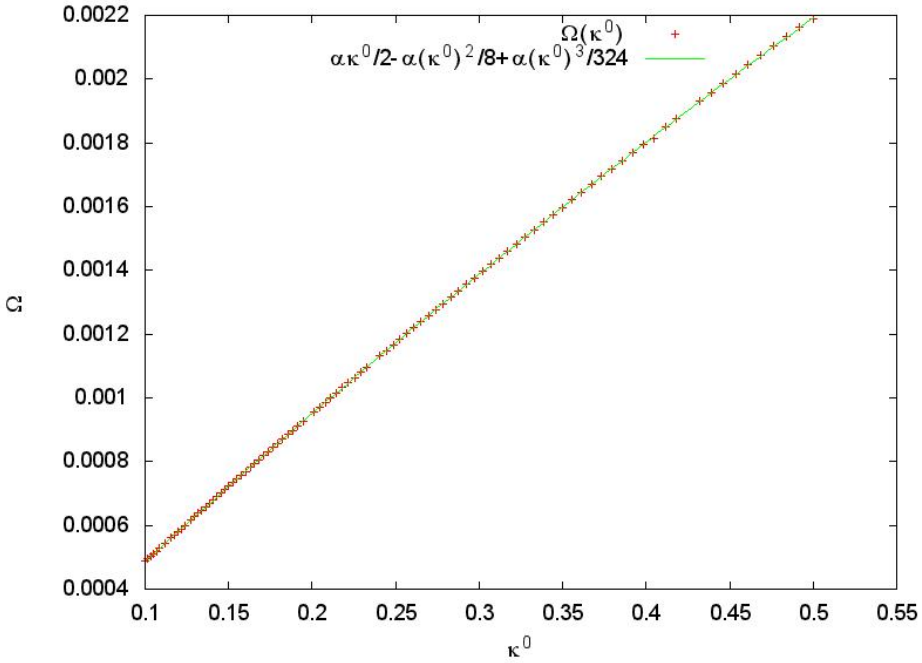

Figure 8: The figure displays in red the values of Ω for a given κ^0 (with $\alpha = \frac{1}{100}$) found by using numerical continuation of a sequential periodic orbit with winding number $\omega = \frac{2\pi}{3}$, that started from the linear elliptic *fixed* points. The overlapped green line correspond to parameter relation (46) found with normal forms.

numerical method. Figure 8 (resp. 9) shows the evaluation of (46) (resp. (47)) using the numerical values of κ versus the numerical value of Ω, the figures show a very good match of the numerical procedure and the normal forms. In this form we obtain very good agreement of the numerics and the asymptotic procedures using normal forms for the case of sequential periodic orbits.

The numerical computations shows that $\Delta\kappa \simeq \frac{\alpha^2}{40}(\kappa^0)^4$ for linear hyperbolic fixed points, which is of the order of the asymptotic result $\Delta\kappa \simeq \frac{\alpha^2}{64}(\kappa^0)^4$ from (48).

A conclusion that we obtain of the use of normal forms is that the sequential periodic orbits that we have constructed, have associated values $\bar{\kappa}$ and $\Delta\kappa$ as functions of the parameters Ω and γ. This is a possible explanation of why the mean field variable κ achieves a mean value and oscillates, at least for this sequential periodic orbit scenario.

In a more general dynamic, we could picture that the oscillatory evolution of the variable κ is driven by a set of orbits close to periodic orbits, periodic orbits associated to the parameters of the evolution. Due this hypothesis, we are interested in studying the frequency space of κ for long times. We hope to perform this analysis in a future work.

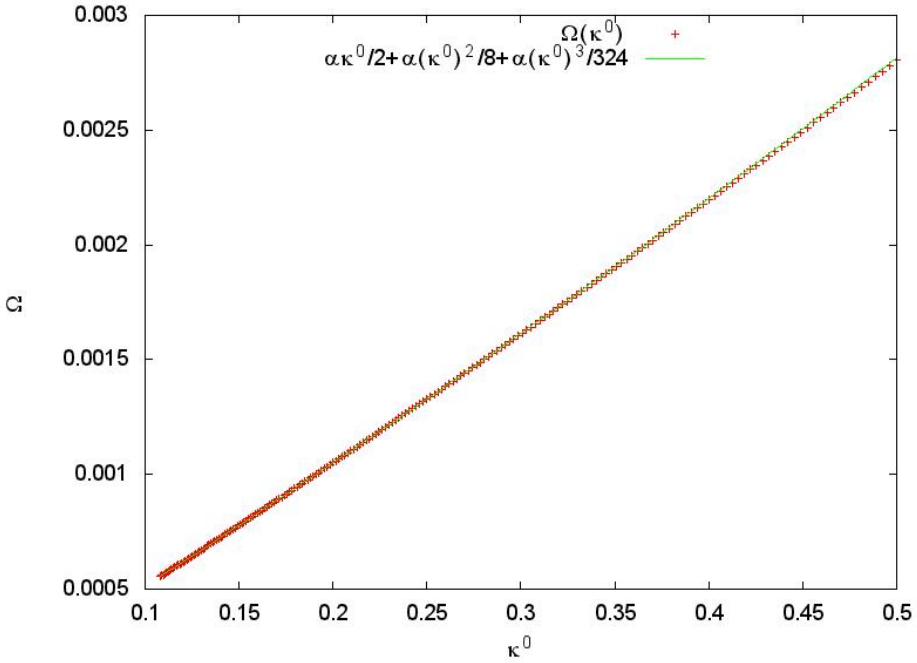

Figure 9: The figure displays in red the values of Ω for a given κ^0 (with $\alpha = \frac{1}{100}$) found by using numerical continuation of a sequential periodic orbit with winding number $\omega = \frac{2\pi}{3}$, that started from the linear hyperbolic *fixed* points. The overlapped green line correspond to parameter relation (47) found with normal forms.

6 Conclusions

In this paper we studied self-consistent chaotic transport in a mean-field Hamiltonian model. The model consists of $N \gg 1$ coupled area-preserving twist maps in which the amplitude and phase of the perturbation (rather than being constant like in the standard map) are dynamical variables. The model provides a simplified description of transport in marginally stable systems including vorticity mixing in strong shear flows and electron dynamics in plasmas.

Of particular interest was the study of coherent structures and periodic orbits. Numerical simulations showed that self-consistency leads to the formation of a coherent macro-particle trapped around the elliptic fixed point of the system, accompanied by an oscillatory behavior of the mean field. To study in detail the transport properties of the self-consistent map in this case, we introduced a non-autonomous standard map in which the amplitude of the perturbation alternates between two values, κ_1 and κ_2 mimicking the observed oscillatory behavior of the mean field in the full self-consistent map.

A turnstile-type mechanism that allows transport across instantaneous KAM invariant circles in non-autonomous systems was presented. This mechanism explains how, contrary to intuition, orbits in the non-autonomous standard map can cross the golden-mean torus even though the values of κ_1 and κ_2 might be below the critical threshold for the destruction of the golden mean torus in the standard map κ_c. This result raises the question of the critical κ_1 and κ_2 parameter values for the onset of global transport (i.e. complete absence of KAM invariant circles) in the non-autonomous standard map. We approached this question numerically and found the region in the (κ_1, κ_2) for which global transport exits. Interestingly, it was observed that the boundary of this "horn-shaped" region exhibits a cusp singularity at $\kappa_1 = \kappa_2 = \kappa_*$.

Based on Moser's twist theorem, a study of the twist condition in the non-autonomous standard map in Eq. (19) indicates that, for small enough values of κ_1 and κ_2 the map must have invariant circles. That is, there will not be diffusion no matter how many iterations are performed on the map. Moreover, since the same argument can be given for a generalized version of the map (19) with m parameters κ_i, $i = 1, 2..., m$, it is possible to construct a high dimensional system with no diffusion.

We also showed that a type of periodic orbits, refer to as sequential periodic orbits, can be used to explain the behavior of the mean field variables of the self-consistent map. In particular, using normal forms, we showed that for sequential periodic orbits to exists, a specific relationship between the mean-field variables κ^0 and θ^0 and the map parameters γ_k and Ω must hold. This result opens the possibility of predicting the asymptotic values of mean-field variable in the case when the initial condition corresponds to a sequential periodic orbit. Nevertheless, at this moment we are incapable to establish a direct connection between these periodic orbits and the oscillatory behavior observed in figures 2 and 3.

Among the several problems we plan to explore in the future is to determine if one can find periodic orbits that drive the asymptotic dynamics of the mean field variables. In this way, we would be able to estimate the transport of the self-consistent model with the help of the turnstile-type mechanism. Another interesting problem is the study the self-consistent map in the limit of small N. Preliminary results indicate that, using symmetries and conservation laws, for $N = 1$, the 4-dimensional map in Eq. (16) can be reduced to a 2-dimensional map.

Acknowledgments

This work was founded by PAPIIT IN104514, FENOMEC-UNAM and by the Office of Fusion Energy Sciences of the US Department of Energy at Oak Ridge National Laboratory, managed by UT-Battelle, LLC, for the U.S.Department of Energy under contract DE-AC05-00OR22725. We also express our gratitude to the graduate program in Mathematics of UNAM for making the GPU servers available to perform our computations and especially

to Ana Perez for her invaluable help. Finally, we would also like to thank the anonymous referee whose valuable comments have improved the presentation of the paper.

References

[1] Bofetta, G., del Castillo, D., López, C., Pucacco, G., Vulpiani, A.: *Diffusive transport and self-consistent dynamics in coupled maps.* Phys. Rev. E **67**, 026224 (2003).

[2] Calleja, R., de la Llave, R.: *Fast numerical computation of quasi-periodic equilibrium states in 1D statistical mechanics, including twist maps.* Nonlinearity **22**(6), 1311-1336, (2009).

[3] Carbajal, L., del-Castillo-Negrete, D., Martinell, J.J.: *Dynamics and transport in mean-field coupled, many degrees-of-freedom, area-preserving nontwist maps* . Chaos **22**, 1, 013137, (2012).

[4] del-Castillo-Negrete, D.: *Weekly nonlinear dynamics of electrostatic perturbations in marginally stable plasmas.* Phys. Plasmas **5**(11), 3886-3900, (1998).

[5] del-Castillo-Negrete, D.: *Self-consistent chaotic transport in fluids and plasmas.* CHAOS, **10**, 75, (2000).

[6] del-Castillo-Negrete, D.: *Dynamics and self-consistent chaos in a mean field Hamiltonian model.* Chapter in "Dynamics and Thermodynamics of Systems with Long Range Interactions", edited by T. Dauxois, S. Ruffo, E. Arimondo, and M. Wilkens. Lecture Notes in Physics Vol. 602, Springer (2002).

[7] Delshams, A., de la Llave, R.: *KAM Theory and a partial justification of Greene's criterion for nontwist maps*, SIAM J. Math. Anal. 31(6), (2000).

[8] Doedel, E.J.: *Lectures Notes on Numerical Analysis of Nonlinear Equations.* http://cmvl.cs.concordia.ca/auto/notes.pdf (2010)

[9] Greene, J.M.: *A Method for Computing the Stochastic Transition.* J. Math. Phys. **20**, 1183-1201, (1979).

[10] Haragus, M., Iooss, G.: *Local Bifurcations, Center Manifolds, and Normal Forms in Infinite Dimensional Dynamical Systems.* Springer, New York (2011).

[11] Kook, H.T., Meiss, J.D.: *Periodic Orbits for Reversible, Symplectic Mappings.* Physica D **35**; 65-86, (1989).

[12] Meiss, J.D.: *Symplectic maps, variational principles and transport*. Rev. Mod. Phys., **64**(3): 795-848, (1992).

[13] Meyer, K.R., Hall, G.R.: *Introduction to Hamiltonian Dynamical Systems and N-Body Problem*. Springer-Verlag, New York (1992).

[14] Moser, J.: *On invariant curves of area-preserving mappings of an annulus*. Nachr. Akad. Wiss. Göttingen Math.-Phys. Kl. **1**(1) 1-20, (1962).

[15] O'Neil, T.M., Winfrey, J.H., Malmberg, J.H.: *Nonlinear interaction of a small cold beam and a plasma.* Phys. Fluids **14** 1204, (1971).

[16] Olvera, A.: *Estimation of the Amplitude of Resonance in the General Standard Map*. Exp. Math. **10**(3); 401-418, (2001).

$1/q$	
$1/2$	$g(\zeta^0,\kappa^0) = \frac{\kappa^0}{4}\sin(\phi^0) + \frac{\alpha(\kappa^0)^2}{32}\left(\cos(\phi^0) - \cos(3\phi^0)\right) - \frac{(3-\alpha^2)(\kappa^0)^3}{512}\sin(\phi^0) + \frac{(1+\alpha^2)(\kappa^0)^3}{512}\sin(3\phi^0) - \frac{\alpha^2(\kappa^0)^3}{512}\sin(5\phi^0) + \mathcal{O}((\kappa^0)^4)$ $\zeta^1 - 2\zeta^0 + \zeta^{-1} = -\frac{(\kappa^0)^2}{a}\sin(2\phi^0) + \frac{\alpha(\kappa^0)^3}{32}\left(\cos(4\phi^0) - 1\right) + \mathcal{O}((\kappa^0)^4)$ *Elliptic:* $\Omega = \mathcal{O}((\kappa^0)^4)$ *Hyperbolic:* $\Omega = \frac{\alpha\kappa^0}{2} - \frac{\alpha(\kappa^0)^2}{64}(1+\alpha^2) + \frac{3\alpha(\kappa^0)^3}{128} + \mathcal{O}(\alpha(\kappa^0)^4)$
$1/3$	$g(\zeta^0,\kappa^0) = \frac{\kappa^0}{3}\sin(\phi^0) + \frac{(\kappa^0)^2}{18}\sin(2\phi^0) + \frac{(\kappa^0)^3}{216}\sin(\phi^0) + \frac{\alpha(\kappa^0)^3}{48}\big(\cos(2\phi^0) - \cos(4\phi^0)\big) + \mathcal{O}((\kappa^0)^4)$ $\zeta^1 - 2\zeta^0 + \zeta^{-1} = -\frac{(\kappa^0)^3}{24}\sin(3\phi^0) + \mathcal{O}((\kappa^0)^4)$ *Elliptic:* $\Omega = \frac{\alpha\kappa^0}{2} - \frac{\alpha(\kappa^0)^2}{8} + \frac{\alpha(\kappa^0)^3}{324} + \mathcal{O}(\alpha(\kappa^0)^4)$ *Hyperbolic:* $\Omega = \frac{\alpha\kappa^0}{2} - \frac{\alpha(\kappa^0)^2}{8} + \frac{\alpha(\kappa^0)^3}{324} + \mathcal{O}(\alpha(\kappa^0)^4)$
$1/6$	$g(\zeta^0,\kappa^0) = \kappa^0\sin(\phi^0) + \frac{(\kappa^0)^2}{6}\sin(2\phi^0) - \frac{7(\kappa^0)^3}{24}\sin(3\phi^0) + \frac{(\kappa^0)^3}{96}\sin(3\phi^0) - \frac{43(\kappa^0)^4}{576}\sin(2\phi^0) + \frac{17(\kappa^0)^4}{576}\sin(4\phi^0) + \frac{25(\kappa^0)^5}{288}\sin(\phi^0) - \frac{185(\kappa^0)^5}{1152}\sin(3\phi^0) + \frac{51(\kappa^0)^5}{384}\sin(5\phi^0) + \frac{211(\kappa^0)^6}{864}\sin(2\phi^0) - \frac{4227(\kappa^0)^6}{34560}\sin(4\phi^0) + \frac{1077\alpha(\kappa^0)^6}{3840}\left(\cos(7\phi^0) - \cos(5\phi^0)\right) + \mathcal{O}((\kappa^0)^7)$ $\zeta^1 - 2\zeta^0 + \zeta^{-1} = -\frac{1077(\kappa^0)^6}{3840}\sin(6\phi^0) + \mathcal{O}((\kappa^0)^7)$ *Elliptic:* $\Omega = \alpha\kappa^0 + \frac{9}{24}\alpha(\kappa^0)^3 - \frac{379}{1151}\alpha(\kappa^0)^5 + \frac{1077}{3840}\alpha(\kappa^0)^5 + \mathcal{O}((\kappa^0)^7)$ *Hyperbolic:* $\Omega = \alpha\kappa^0 + \frac{9}{24}\alpha(\kappa^0)^3 - \frac{379}{1151}\alpha(\kappa^0)^5 - \frac{1077}{3840}\alpha(\kappa^0)^5 + \mathcal{O}((\kappa^0)^7)$

Table 1: Normal forms for some sequential periodic orbits with ration rotation numbers. In the table we display: (i) the change of variables g, (ii) the resonant normal form and needed parameter relations for (iii)*elliptic* and (iv)*hyperbolic* fixed points.